General Disclaimer

One or more of the Following Statements may affect this Document

- This document has been reproduced from the best copy furnished by the organizational source. It is being released in the interest of making available as much information as possible.

- This document may contain data, which exceeds the sheet parameters. It was furnished in this condition by the organizational source and is the best copy available.

- This document may contain tone-on-tone or color graphs, charts and/or pictures, which have been reproduced in black and white.

- This document is paginated as submitted by the original source.

- Portions of this document are not fully legible due to the historical nature of some of the material. However, it is the best reproduction available from the original submission.

JPL PUBLICATION 78-44

Preliminary Studies of Electromagnetic Sounding of Cometary Nuclei

Andrew Gabriel
Larry Warne
Steven Bednarczyk
Charles Elachi

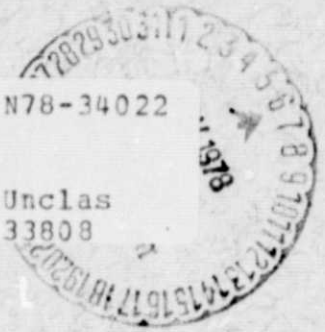

October 1, 1978

National Aeronautics and
Space Administration

Jet Propulsion Laboratory
California Institute of Technology
Pasadena, California

JPL PUBLICATION 78-44

Preliminary Studies of Electromagnetic Sounding of Cometary Nuclei

Andrew Gabriel
Larry Warne
Steven Bednarczyk
Charles Elachi

October 1, 1978

National Aeronautics and
Space Administration

Jet Propulsion Laboratory
California Institute of Technology
Pasadena, California

The research described in this publication was carried out by the Jet Propulsion Laboratory, California Institute of Technology, under NASA Contract No. NAS7-100.

PREFACE

The work described in this report was performed by the Telecommunications Science and Engineering Division of the Jet Propulsion Laboratory.

ACKNOWLEDGMENT

Larry Warne is currently with Sandia Laboratories, Albuquerque, New Mexico. The Electromagnetic Sounding of Cometary Nuclei Team consists of Drs. C. Elachi and M. Kobrick (Jet Propulsion Laboratory), C. H. Papas (California Institute of Technology), J. Veverka (Cornell University) and G. Wetherill (Carnegie Institute). Discussions between the team members formed the key inputs to this report. Support from all of the team members is gratefully acknowledged. The authors also thank Professor P. Gudmandsen, from the Technical University of Denmark, for providing Figure 2-2.

ABSTRACT

The structure of cometary nuclei is a key issue in solar system cosmogony. The internal structure of a comet could be determined with a spacecraft borne electromagnetic sounder. A dielectric profile of the comet could be produced in direct analogy with terrestrial glacier and ice sheet sounding experiments. This profile would allow the detection of a rocky core or ice layers if they exist, just as layers in the ice and the bedrock interface have been clearly observed through the Greenland ice sheet. It would also provide a gross estimate of the amount of dust in the icy region. Models for the response of the nucleus and cometary plasma to electromagnetic sounding are developed and used to derive experimental parameters. A point system design was completed. Preliminary engineering study results indicate that the sounder is well within the bounds of current space technology.

CONTENTS

Figures

Tables

SECTION I

INTRODUCTION

The origin and structure of comets is a key issue in solar system cosmogony. One theory suggests that comets are in fact nearly unaltered samples of the primordial material from which the sun and planets accreted, and hence, bear information about the conditions extant 4.5 billion years ago when the solar system was formed. Alternatively, it is possible that comets contain material from the interstellar medium and may predate the solar system (Report of the Comet Halley Science Working Group, 1977). Comets are known to contain organic molecules (Ip and Mendis, 1976); these molecules may have played important roles in forming the very early environments of all the planets. Additionally, what relation comets have to asteroids and meteorites, aside from well-known orbital similarities, is unknown. It is possible that asteroids and meteor streams are defunct comets, long since stripped of whatever volatile ingredients give comets their spectacular appearance. Since current theories of the solar system's origin are based in part on data from these asteroids, what relation they have to comets is a question of paramount importance.

Current knowledge of comets is quite scarce, and is based almost solely on spectroscopic analysis of light emanating from the coma and tail. These data have allowed tentative identification of various organic-free radicals (Ip and Mendis, 1976; Whipple and Heubner, 1976) and considerable speculation about the molecular origins thereof. Some theoretical models covering physical ionization processes in the coma and the interaction of the coma with the solar wind have been attempted, but there is no direct information on the size, structure and composition of comets' nuclei and the cometary plasmas, and hence these models are somewhat speculative.

The cometary model with the widest endorsement is undoubtedly that of Whipple (Whipple, 1950). A comet is postulated to consist of a large nucleus made of rocks with substantial amounts of accreted ice, typically several kilometers across. There may be large quantities of impurities, dust and chemical matter imbedded in the ice. In this model, when a comet approaches the sun, the nuclear ice starts to sublime and ionize, thereby dispersing dust and molecules, which are blown by the solar wind to form the cometary tails.

Direct missions to comets are needed to finally solve some of the key problems in cometary structure research (Report of the Comet Halley Science Working Group, 1977) such as: Verify that a solid nucleus exists at all, and if it does exist, what is its size? What is the nature of the nuclear ice? Does the nucleus have one large rocky core, a collection of smaller rocks and dust embedded in ice, or some combination of the two? If there is a core, what is its size and shape?

The objective of this report is to discuss the potential of a spaceborne electromagnetic sounder to answer some of these questions and to evaluate the feasibility of such a sensor.

SECTION II

ELECTROMAGNETIC SOUNDING OF THE NUCLEUS

Deep electromagnetic sounding of the nucleus from a nearby location (i.e., less than a few tens of kilometers) could unambiguously resolve some of the key questions about nuclear structure; in particular, the presence or absence of a rocky core and its size, the presence of layering in the ice, and the spatial distribution and amount of rocks and dust in the icy region of the nucleus.

Electromagnetic sounding of a solid nucleus is, at least in principle, very simple. An antenna launches a short-pulsed electromagnetic wave aimed at the nucleus. The wave propagates through space and strikes the nuclear surface. Part of the wave is transmitted, and part is reflected. The transmitted wave continues to propagate through the nucleus and is reflected by any macroscopic change in the dielectric constant. Thus, a rock-ice interface or a large center of impurities will cause some reflection. Meanwhile, the antenna is switched into a receiving mode and will detect any radiation that is reflected back. The first return will come from the surface interface; later returns will come from scattering centers and interfaces inside the nucleus, and there may be some reflected radiation from the rear surface interface (Figure 2-1). By probing from different locations around the nucleus, a three-dimensional "map" of the internal structure may be deduced.

Sounding techniques have been developed for terrestrial glaciers and ice sheet mapping (Gudmandsen, 1975, 1976; Robin et al., 1969; Hockstra and Capillino, 1971; Evans, 1965). Sounding of Greenland and Antarctic ice sheets, down to the bedrock through many kilometers of ice, has been achieved with airborne electromagnetic sounders (Figure 2-2) using a reasonably low amount of power which is compatible with spacecraft capabilities. Numerous layers have been observed throughout these ice sheets. Water ice is nearly transparent for electromagnetic radiation at frequencies between 0.1 and 100 MHz (Figure 2-3). Waves launched at these frequencies will propagate with little loss through the ice and reflect from rocks, bubbles, dislocations and finally from the underlying bedrock. The time separation between the reflections from the surface and bedrock interfaces allows the determination of the ice thickness assuming that the real part of the ice dielectric constant is reasonably well known. As the sensor platform moves above the surface of the ice, a complete profile of the internal structure is obtained.

The extension of the above method to the sounding of a comet nucleus is straightforward; the principal component of nuclear material is expected to be water ice (Ip and Mendis, 1976), so the above conclusions about propagation through glacial ice sheets hold reasonably well. The effect of dust in the cometary ice will be discussed later in some detail. The radio sounder could measure the size of the nucleus and determine whether or not it has a core. Sounding could determine the approximate value of the dielectric constants of the surficial and internal material. By probing the nucleus from many different directions, the location of small rocks, dust patches and other scattering centers might be determined in direct analogy with glacier sounding.

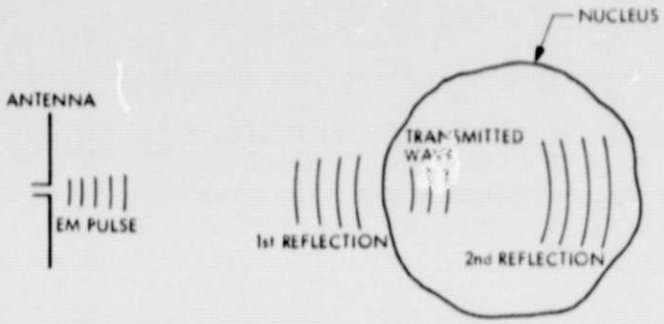

Figure 2-1. Specular Return from the Nucleus. Electromagnetic waves launched from the antenna are reflected and transmitted at the surface of the nucleus (front interface). The transmitted energy propagates through the nucleus and is reflected at its back surface.

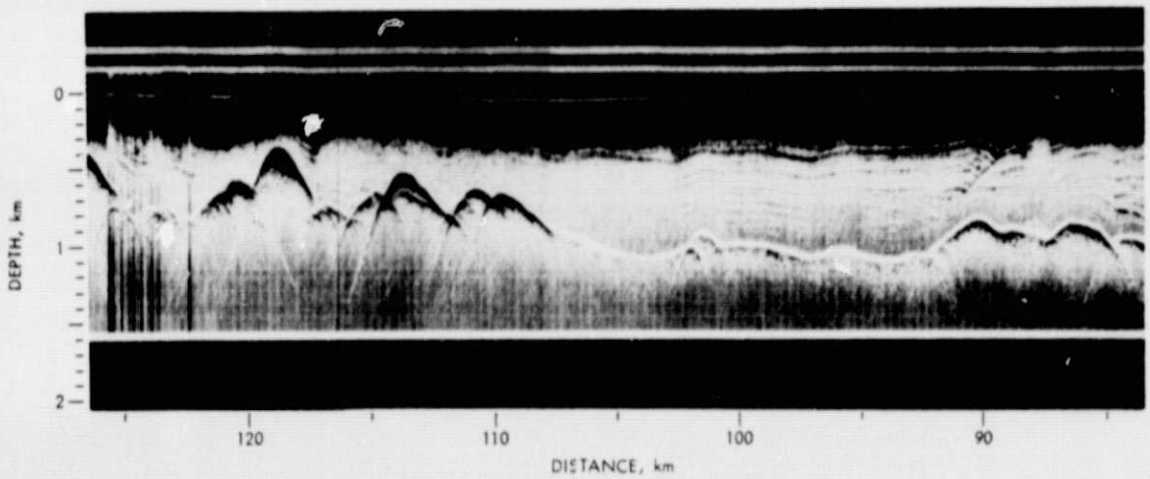

Figure 2-2. Internal Structure of Greenland Ice Sheet. The flight track of a plane carrying an electromagnetic sounder corresponds to the horizontal axis. Depth is on the vertical axis. Layers and the bedrock interface are clearly seen. Sounding to a depth of more than 3 km has been reported. The sounder frequency is 60 MHz. (Courtesy of the Electromagnetic Institute, Technical University of Denmark.)

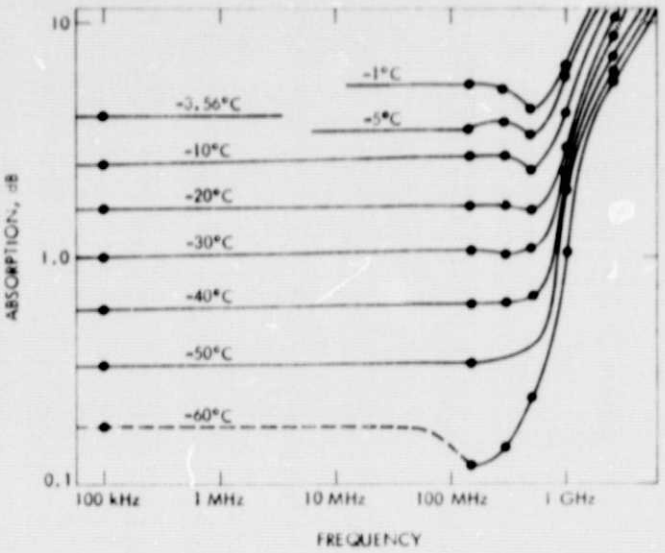

Figure 2-3. Attenuation of Electromagnetic Waves in Ice. Absorption per 100 m is given as a function of frequency, with temperature as a parameter (from Smith and Evans, 1968).

SECTION III

FREQUENCY SELECTION

The amplitude of the signal backscattered from the nucleus will almost inevitably be reduced many orders of magnitude from the amplitude of the transmitted radiation. Compounded with limited power typical of spacecraft sensors, this means the sounder must be designed to maximize the returned signal. It is particularly important that the antenna has a high directivity gain and that the transmitted radiation is nowhere evanescent in the cometary plasma.

This latter requirement immediately precludes sounding the nucleus with low frequency radiation. In particular, electromagnetic waves will not propagate through the plasma at frequencies below the plasma frequency, ω_p:

$$\omega_p^2 = \frac{4\pi ne^2}{m} \qquad (3\text{-}1)$$

where

n = electron density

m = electron mass

e = electronic charge

In a cometary plasma, the maximum electron density will occur at perihelion, when the nuclear ice is sublimated at a maximum rate. According to Ip and Mendis (1976), a typical peak electron density at a 1 AU perihelion for a 5-km nucleus on the sunward side is 10^5 cm^{-3}. Since observed plasma isophotes are approximately elliptical (Feldman, 1977), it is reasonable to conclude that the peak electron density is not any lower on the dark side of the nucleus.

The plasma frequency corresponding to an electron density of 10^5 cm^{-3} is approximately 10^7 Hz (i.e., 10 MHz). This may be regarded then as an overall lower limit on the sounding frequency from any sounding position around the nucleus.

Higher sounding frequencies are advantageous because they require smaller antennas; however, care must be taken that the attenuation of the wave in the ice does not become too severe (Figure 2-3), and that scattering by rocks with a size of a fraction of a meter or less does not attenuate the wave excessively. The above factors indicate that a sounding frequency range of 30 to 100 MHz is the most desirable.

The impurities in the nuclear ice are most probably ammonia, methane, carbon dioxide, and dust (Feldman, 1977; Whipple and Heubner,

1976). It is also possible that more exotic molecules are present, but only in trace amounts, too small to affect the propagating electromagnetic wave. Ammonia, methane, and carbon dioxide, even if they are quite abundant, will only marginally change the refractive index of water ice (Westphal, 1977) and may be ignored in preliminary calculations. It is a reasonable assumption that no compounds with anomalous dielectric behavior are formed from these impurities. Dust, however, may increase the dielectric constant in the nucleus substantially; there may be as much as a factor of two difference between the real dielectric constant of ice and that of dirty ice with silicates or "rocks." The effect of dust concentration on the electromagnetic waves is modeled in the next section.

SECTION IV

MODELS PREDICTING THE RETURNED SIGNAL

A number of phenomena would result in a returned echo as the incident electromagnetic wave propagates through the nucleus:

(1) The wave is reflected at the front surface of the nucleus, at any interface (such as layers in the ice or on the surface of a rocky core) throughout the nucleus, and at the back surface of the nucleus (see Figures 2-1 and 4-1a). As it propagates through the nucleus, the wave is attenuated by absorption in the ice, the dust and the impurities and scattered from rocky fragments.

(2) The wave can be refracted and returned back to the antenna. This is somewhat similar to the "halo" effect and Luneberg lens effect (see Figure 4-1b).

(3) The wave can be backscattered from any roughness on the surface of the nucleus (see Figure 4-1c).

Other phenomena can also occur, such as surface waves which would circumnavigate the nucleus and re-radiate back toward the antenna (Figure 4-1d). However, in this preliminary report we will only consider, in a simplified fashion, the first three phenomena listed above, which seem to be the most important.

A. REFLECTION AND ABSORPTION

Backward reflection occurs when a wave is normally incident on an interface where there is a change in the dielectric constant. The exact calculation of the backward reflection from a layered dielectric sphere is somewhat involved. However, a planar layered medium can be used (see Figure 4-2) to obtain a first-order estimate of the echos from the different interfaces in the nucleus.

In the case of a homogeneous nucleus (Figure 4-2a), the power P_r of the echo reflected by the front surface is equal to

$$P_r = \frac{P_t G A r_1}{16\pi(d - a)^2} \qquad (4\text{-}1)$$

where

P_t = transmitted power

G = antenna gain

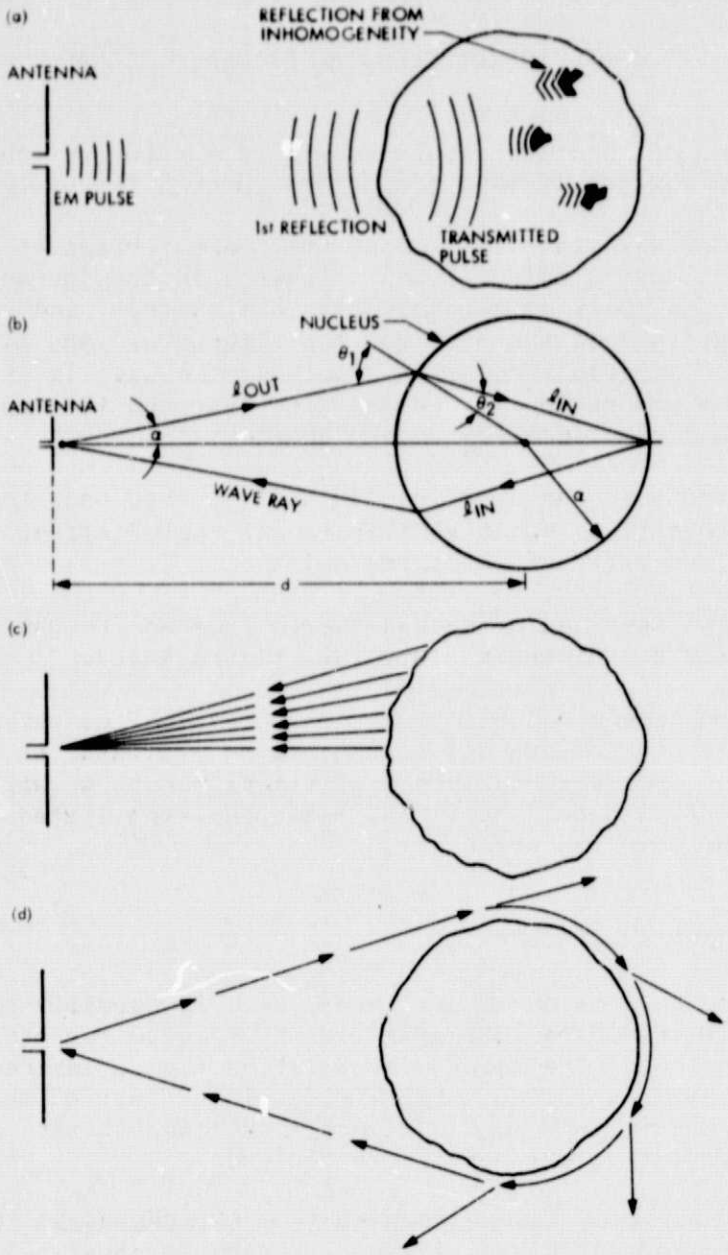

Figure 4-1. Phenomena Causing an Echo. (a) Reflection and scattering from internal inhomogeneities including layers, large core or relatively small-scale inhomogeneities. (b) Uniquely refracted modes where the wave path is refracted inside the nucleus and returned straight back to the source. (c) Back-scattering from the surface roughness. (d) Surface waves which would propagate all around the nucleus.

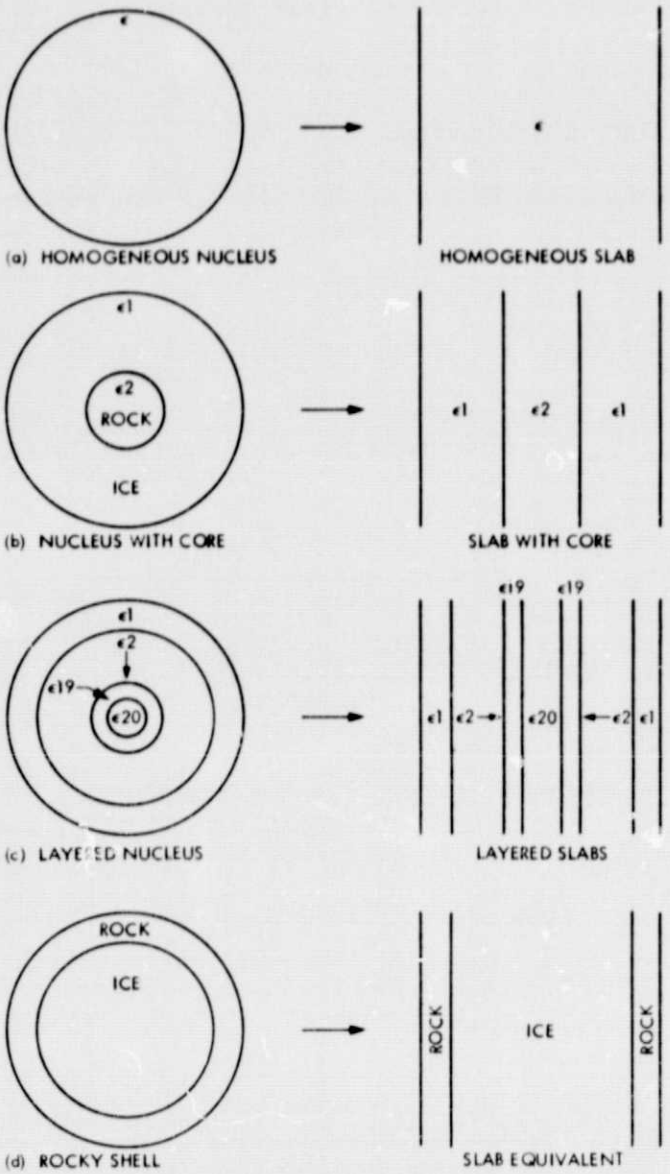

Figure 4-2. Nuclear Models and Corresponding Planar Models. (a) Homogeneous nucleus of ice (including dirty ice). (b) Nucleus with a rocky core. (c) Layered nucleus. (d) Nucleus with a rocky crust and an icy core.

A = antenna effective receiving area

d = distance to the center of the nucleus

a = radius of the nucleus

r_1 = Fresnel reflection coefficient of the surface

$$= \left[\frac{\sqrt{\epsilon} - 1}{\sqrt{\epsilon} + 1}\right]^2$$

The power of the echo from the back surface is equal to

$$P_r' = P_r \frac{GAr_2\gamma T^2}{16\pi\left[d + \left(\frac{2}{\sqrt{\epsilon}} - 1\right)a\right]^2} \qquad (4\text{-}2)$$

where

T = transmittivity of the first interface

γ = roundtrip attenuation factor for the nucleus material

r_2 = reflectivity of the second interface

Of particular interest is the power ratio of the two echos:

$$\frac{P_r'}{P_r} = \left[\frac{d - a}{d + \left(\frac{2}{\sqrt{\epsilon}} - 1\right)a}\right]^2 T\alpha \qquad (4\text{-}3)$$

In the above expression, we took $r_1 = r_2$. This ratio is plotted in Figure 4-3 for different values of d/a and for $\epsilon = 3.2$ which is the dielectric constant of water ice. This ratio represents the strength of the echo from the back side of the nucleus versus the echo from the front side. In other terms, it is the capability of seeing all through a homogeneous nucleus. To illustrate, let us assume that d/a = 4, a = 2.5 km and the absorption in the ice is 3 dB/km. Then we have

$$\frac{P_r'}{P_r} = -33 \text{ dB}$$

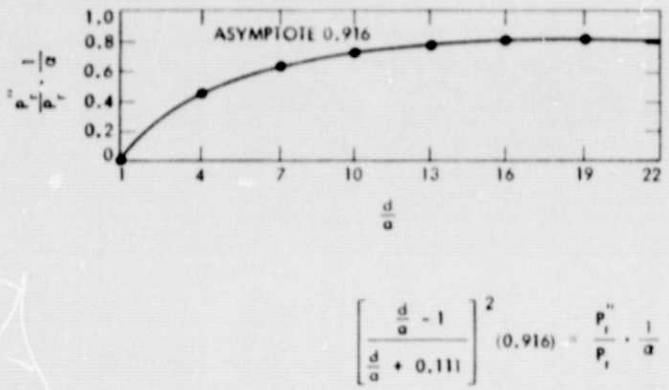

$$\left[\frac{\frac{d}{a}-1}{\frac{d}{a}+0.111}\right]^2 (0.916) = \frac{P_r''}{P_r} \cdot \frac{1}{a}$$

Figure 4-3. Echoes from Front and Rear Nuclear Surfaces. Ratio of power return from the back interface (P_r'') and front interface of the nucleus (P_r) versus the ratio of the distance of the spacecraft from nucleus center (d) to nuclear radius 'a). The roundtrip absorption in the nucleus is a.

Thus, if we impose that the backside echo must have a signal-to-noise ratio (SNR) of at least 13 dB, then the front side echo must have an SNR of 46 dB.

In the case of a rocky core (Figure 4-2b) of radius R_c, the power ratio of the echoes from the nucleus surface and the rocky core surface is simply equal to

$$\frac{P_r''}{P_r} = \left[\frac{d-a}{d+\left(\frac{2}{\sqrt{\epsilon}}-1\right)\left(\frac{a-R_c}{2}\right)}\right]^2 \frac{\sqrt{3}}{r_1} T a \qquad (4\text{-}4)$$

where r_3 is the reflectivity at the ice-rock interface.

This ratio is plotted in Figure 4-4 for a rocky core of dielectric constant equal to 7 which is typical of silicate materials. The echoes from the back surface of the core and nucleus are expected to be very weak because of the absorption which occurs as the wave propagates through the rocky core itself.

If we assume that the core has a 1-km radius, then using the same parameters as above, we find

$$\frac{P_r''}{P_r} = -12 \text{ dB}$$

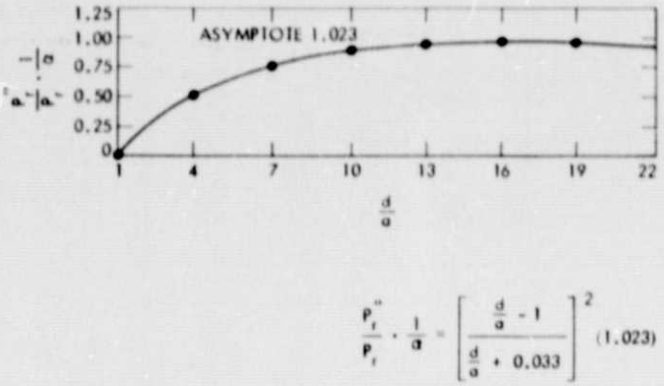

$$\frac{P_r''}{P_r} \cdot \frac{1}{\alpha} = \left[\frac{\frac{d}{a} - 1}{\frac{d}{a} + 0.033}\right]^2 (1.023)$$

Figure 4-4. First Echoes from Nuclear Surface and Core. Ratio of power return from the core-ice interface (P_r'') and the nucleus surface (P_r). The roundtrip absorption in the ice crust is α.

Thus, if we impose a minimum SNR of 13 dB for the echo from the core, then the front side echo must have an SNR of 25 dB.

The SNR imposed on the front echo defines the parameters and performance of the sensor. In Table 4-1 we give the parameters of a point design sensor which is well within the present state-of-the-art of space technology. To illustrate the performance of such a sensor, let us assume d = 10 km. Then

$$SNR = \frac{P_r}{kTB} = 80 \text{ dB}$$

where P_r is given in Equation (4-1). This gives a very high SNR, which means that sounding could be easily accomplished from even farther distances. This will be discussed later.

It is possible that each time a comet passes through perihelion, only the volatiles in the icy mantle are stripped off, and that dust and rocks are left behind. Particularly in an older comet, this could lead to a "rocky shell" effect (Figure 4-2d), where a high concentration of rocks and dust remain near the surface of the nucleus with an icy core at the center. Using the sensor parameters in Table 4-1, the SNR predicted for the echoes from an equivalent slab model (Figure 4-2d) is shown in Figure 4-5. The SNR was calculated for the case where the spacecraft is 10 km away from the surface of the nucleus. It is clear that even with a 1-km thick crust, complete sounding can still be achieved from a 10-km range.

Table 4-1. System Parameters

Parameter	Value
Frequency	f = 40 MHz
Wavelength	λ = 7.5 m
Peak Power Transmitted	P_t = 500 W
Pulse Length	5 μs
Bandwidth	B = 2 MHz
Range Resolution	75 m in free space
	45 m in ice
Pulse Repetition Frequency (PRF)	10
Average Transmitted Power	0.1 W
Receiver Noise	T = 600 K
Antenna	Yagi (3 dipole elements, each 1.9 m long); main lobe has azimuthal symmetry
Antenna Gain	G = 6 dB

The most general case consists of a large number of layers with a continuously increasing dielectric constant toward the center of the nucleus (Figure 4-2c). This case can be easily simulated if the curvature effects of the incident wave and the nucleus are neglected. Figure 4-2c illustrates one case where the dielectric constant varies linearly in 20 layers from ϵ = 3.2 at the nucleus surface to ϵ = 4 at the nucleus center. Figure 4-6 shows the SNR for reflection from this layered slab model, where the envelope of the peaks from the successive interfaces is plotted.

B. EFFECTS OF DUST AND IMPURITIES

To study the effects of impurities we calculated the change in the dielectric constant of ice when impurity with a different dielectric constant is added. The resulting composite dielectric constant is given by (Von Hippel, 1954)

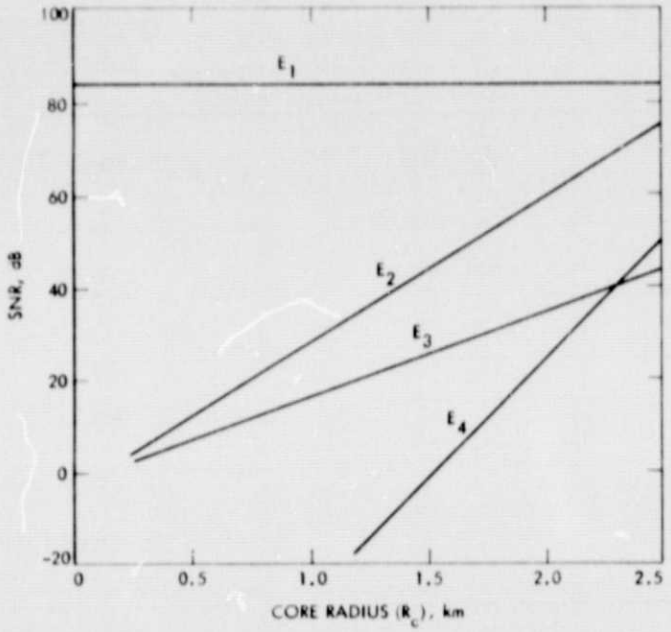

Figure 4-5. First and Second Echoes from the Nuclear Surface and Core. Signal-to-noise ratio of the echoes from the four interfaces which correspond to a nucleus with an icy core and a rocky shell. The sounder is 10 km away from the nucleus. E_1 corresponds to the echo from the front surface. E_2 is for the echo from the front rock-ice interface. E_3 is for the echo from the back ice-rock interface. E_4 is for the back surface. R_c is the core radius.

$$\log \epsilon = p \log (\epsilon_{imp}) + (1 - p) \log (\epsilon_{ice}) \qquad (4\text{-}5)$$

where

ϵ = composite dielectric constant
p = impurity concentration by volume
ϵ_{imp} = impurity dielectric constant
ϵ_{ice} = ice dielectric constant

The composite dielectric constant for various impurity dielectric constants is shown as a function of impurity concentration p in Figure 4-7.

Additionally, impurities affect the absorption properties of ice. The attenuation of the power of the wave in a lossy medium due to Rayleigh absorption by tiny distributed scattering centers is given by (Battan, 1972)

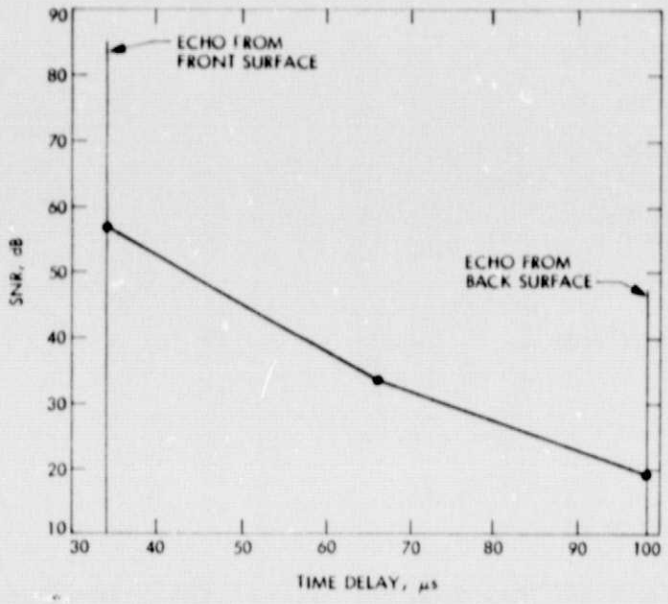

Figure 4-6. Signal-to-Noise Ratio for a 20-Layer Nucleus. The curve is the envelope of the echoes from each interface. The horizontal axis is the time between the transmitted signal and received echo. The sharp rises at 34 μs and 98 μs correspond to the echoes from the front and back surfaces respectively. The sounder is 10 km from the nucleus.

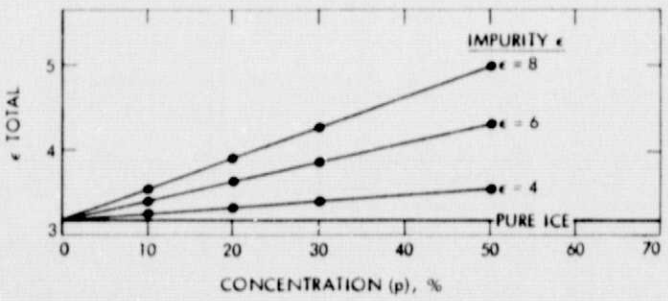

Figure 4-7. Dielectric Constant of Ice with Impurities. The dielectric constant of ice is plotted as a function of impurity concentration (by volume) for different types of impurities. Curve A corresponds to $\epsilon_i = 4$, $\tan \delta_i = 10^{-3}$; curve B corresponds to $\epsilon_i = 5$, $\tan \delta = 10^{-2}$; curve C corresponds to $\epsilon_i = 8$, $\tan \delta = 10^{-1}$; curve D corresponds to $\epsilon_i = 10$, $\tan \delta = 10^{-1}$.

$$P_r = P_{ro} e^{-2NQ_a r} \tag{4-6}$$

where

P_r = power at distance r
P_{ro} = initial power
N = number of lossy scatterers/m^3
r = distance into medium

$$Q_a = 4\pi ka^3 \, \mathrm{Im}\left[-\frac{m^2 - 1}{m^2 + 2}\right]$$

k = $2\pi/\lambda$, λ = wavelength
a = scatter size
m = index of refraction (square root of dielectric constant) of scatterer

The standard form for attenuation by a slightly lossy medium is

$$\exp\left(2ki\sqrt{1 + i \tan\delta}\right) \approx \exp\left[2ki\left(1 + \frac{i \tan\delta}{2}\right)\right]$$

where tan δ is the loss tangent of the medium. Equating the real parts of the exponents, we obtain the equivalent loss tangent

$$\tan\bar{\delta} = -8\pi Na^3 \, \mathrm{Im}\left[-\frac{m^2 - 1}{m^2 + 2}\right]$$

We also have

$$\mathrm{Im}\left[-\frac{m^2 - 1}{m^2 + 2}\right] \approx \frac{3\epsilon''}{(\epsilon' + 2)^2} = -\frac{3\epsilon'}{(\epsilon' + 2)^2} \tan\delta_{imp}$$

where $\tan\delta_{imp} = \epsilon''/\epsilon'$

Thus

$$\tan\bar{\delta} = p \frac{18\epsilon'}{(\epsilon' + 2)^2} \tan\delta_{imp} \tag{4-7}$$

where p is the percentage of impurities by volume. This expression gives the loss tangent due to impurities. The total equivalent loss tangent also includes the absorption in the ice matrix. This gives

$$\tan \bar{\delta} = (1 - p) \tan \delta_{ice} + p \frac{18\epsilon'}{(\epsilon' + 2)^2} \tan \delta_{imp} \qquad (4\text{-}8)$$

A plot of tan $\bar{\delta}$ for various values of impurity concentration is given in Figure 4-8. For comparison, we give in Table 4-2 the values of tan δ for a number of minerals encountered on Earth.

To evaluate the effect of dust concentration on the capability of sounding the nucleus, let us consider the case of a homogeneous dirty ice nucleus. We plotted in Figure 4-9 the SNR of the echo from the back of the nucleus (i.e., opposite side from the spacecraft) as a function of the loss tangent. If we assume a minimum SNR of 13 dB, then the equivalent loss tangent must be lower than 1.1×10^{-3}. This sets an upper limit on the amount of impurity which would still allow sounding of the entire nucleus (from Figure 4-8).

If there are well-defined layers, the returned signal would have a number of well-defined echoes similar to the case of Earth ice sheet sounding (Figure 2-2). As the spacecraft moves around the nucleus, a three-dimensional model would then be obtained about the spatial extent of these layers.

If the nature of the nuclear material changes gradually toward the center, the returned signal would consist of a diffuse echo (as opposed to distinct pulses). The shape of the echo could then be used to deduce information about the internal structure of the nucleus. This latter case would be somewhat harder to interpret exactly.

In actuality, the analysis of the sounding data, which would be obtained during a comet rendezvous mission, is an inverse problem. The internal structure is unknown while the echo characteristics are measurable. The only other relevant information available would be the size of the nucleus (from photography and ranging), some idea about the composition at the surface from analysis of the ejected material and possibly the nuclear mass.

If the nucleus is a homogeneous ice ball (Figure 4-2a), the returned signal would consist of two echoes: one from the front surface and the other from the back surface. The amplitude of the first one would give an approximate value of the dielectric constant at the surface. The time delay between the two echoes and the size of the nucleus would give the average dielectric constant throughout the nucleus, and the relative amplitude of the two echoes would give a gross estimate of the attenuation constant. These measurements, taken together, would give some information about the percentage of impurities and dust in the nucleus.

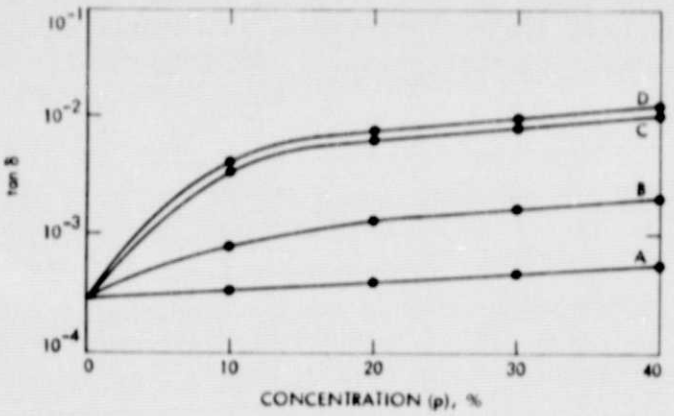

Figure 4-8. Loss Tangent of Ice with Impurities. The loss tangent of ice is plotted as a function of impurity concentration.

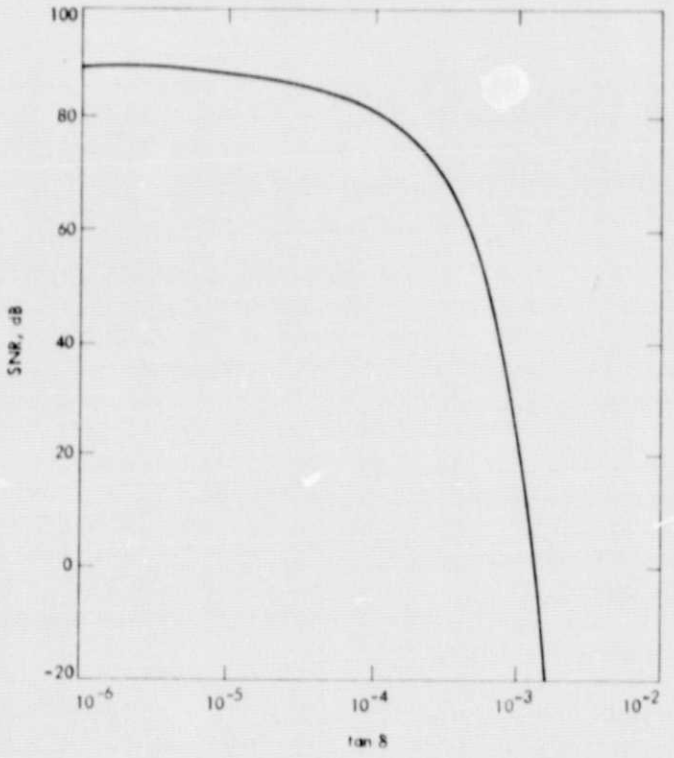

Figure 4-9. Echoes from a Lossy Nucleus Signal-to-noise ratio of the echo from the back side of a dirty ice nucleus as a function of the total loss tangent. It was assumed that 100 echoes were added incoherently. The distance from the spacecraft to the nucleus center is 10 km.

Table 4-2. Loss Tangent of Different Rocks[a]

Rock Type	Tan δ
Plagioclase	3×10^{-3}
Augite	3×10^{-2}
Hypersthene	10^{-3}
Basalt	10^{-2}
Granite	3×10^{-3}
Dunite	3×10^{-3}
Limonite	10^{-3}
Gypsum	5×10^{-4}
Orthoclase	5×10^{-3}
Olivine	10^{-2}
Muscovite	3×10^{-4}
Palagonite	15×10^{-2}
Pyrophyllite	10^{-3}
Chondrites[b]	2×10^{-1} to 2×10^{-2}

[a]From E. I. Prkhamenko, Electrical Properties of Rocks, Plenum Press, New York, 1967.

[b]From The Moon, Edited by Z. Kopal and Z. K. Mikhailov, Academic Press, London, 1962.

If the nucleus has a rocky core, the second echo would appear much closer to the first one than in the case of a homogeneous iceball. The temporal separation between the two echoes would give the thickness of the ice mantle, and therefore the size of the core. The same applies for the case of a rocky crust with any icy core. However, the relative and absolute strength of the successive echoes will be different than in the previous case. This would allow us to identify the actual nature of the core and the crust.

If the nucleus has a large number of layers, then the sounding echoes will be similar to what is shown in Figure 2-2.

C. REFRACTION

Because of the spherical geometry of the nucleus, it is possible that some wave rays get refracted and returned back straight to the antenna (Figure 4-1b). The angles at which this effect occurs can be easily determined. A wavelet emitted at angle α rotates through angle $\theta_1 - \theta_2$ when it refracts, and through angle $\pi - 2\theta_2$ when it reflects. Calling N the number of path segments within the nucleus (e.g., the number of reflections is N - 1) and M the number of times the ray makes a full rotation, then the backward refraction condition is

$$2(\theta_1 - \theta_2) + (N - 1)(\pi - 2\theta_2) = 2\alpha + \pi + 2M\pi \qquad (4\text{-}9)$$

Also, since

$$\sin \theta_1 = \frac{d}{a} \sin \alpha$$

Snell's law gives

$$\frac{d}{a} \sin \alpha = \sqrt{\epsilon} \sin \theta_2$$

Combining the above equations, we obtain the condition for "back to the antenna" refraction:

$$\text{arc sin}\left(\frac{d}{a} \sin \alpha\right) - N \text{ arc sin}\left(\frac{d}{a\sqrt{\epsilon}} \sin \alpha\right) - \alpha + \frac{(N - 2 - 2M)\pi}{2} = 0 \qquad (4\text{-}10)$$

The zeros of this equation, which can be found numerically, give those values of α that will return a signal straight back toward the antenna.

The lengths of the two segments of the signal path are given by (see Figure 4-1b)

$$\ell_{in} = 2a \cos \theta_2 \qquad (4\text{-}11)$$

$$\ell_{out} = -a \cos \theta_1 + \sqrt{d^2 - a^2 \sin^2 \theta_1} \qquad (4\text{-}12)$$

which allows computation of the geometric attenuation.

Calculating the change in attenuation due to changes in the radius of curvature of the pulse is considerably more difficult in this spherical geometry than in the previous slab model. Keeping for the present the approximation that the geometric attenuation is given by the inverse square of the total path length, the returned signal as a function of time may be computed easily. The transmission $T(\theta)$ and reflection $R(\theta)$ are independent of the direction of the ray; that is, a ray refracts through the same angles and is attenuated by the same amount whether it is entering or leaving the nucleus. Therefore, for a given mode (i.e., a certain value of N), the total attenuation is

$$\frac{T^2 R^{N+1}}{4\pi(2\ell_{out} + N\ell_{in})^2} e^{-\delta N \ell_{in}} \qquad (4\text{-}13)$$

where $e^{-\delta N \ell_{in}}$ accounts for the absorption loss throughout the nucleus. R and T are the reflection and transmission coefficients at the surface (Born and Wolf, 1965). The time at which the signal arrives at the antenna is given by

$$\tau = \frac{c}{2\ell_{out} + N\sqrt{\epsilon}\,\ell_{in}} \qquad (4\text{-}14)$$

There are obviously several competing factors in the first expression; when α increases R and N increase, while T decreases. It is not obvious which modes give the strongest return. Computational results (below) show, however, that in general the returned power always decreases as N increases, except when the signal is very strongly attenuated.

The computation involved in determining the refracted signal is not difficult. The basic approach is to iterate α, M, and N in Equation (4-10) and find the zeros; the values of α so obtained correspond to the refracted modes. Then using Equations (4-11) through (4-14), it is straightforward to find θ_2, ℓ_{in}, ℓ_{out}, T, time delay τ, and the total attenuation. The signal-to-noise ratio for four main refracted modes is shown in Figure 4-10. Curve a corresponds to the mode where the wave ray is along the line from the sensor to the nucleus center. Curve b corresponds to the refracted mode shown in Figure 4-1b. Curves c and d correspond to the case where N = 5 and 4 respectively, and M = 1. It is clear that the two first modes are the main contributors to the returned echo.

D. SURFACE BACKSCATTER

The surface of the nucleus is most probably not a perfectly smooth sphere. The surface roughness will backscatter some of the incident energy; however, because the radar wavelength is at least several meters, the surface backscatter contribution is expected to be very small, unless the surface is extremely rough. In any case, such backscattered energy will be received immediately after the specular echo from the front surface. Thus, such echoes will only affect returns from the regions immediately below the surface.

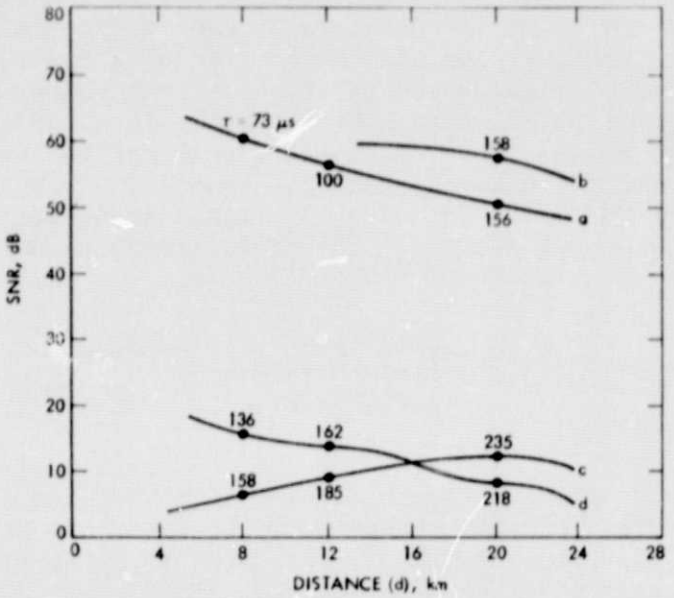

Figure 4-10. Echoes from the Refracted Modes. Signal-to-noise ratio of four main refracted modes as a function of the distance between the sensor and the nucleus center. The nucleus is assumed to have a radius of 2.5 km and the loss in the ice is assumed to be 2 dB/km. Also marked on the curves is the time of arrival of the echoes expressed in μs.

SECTION V

SYSTEM PARAMETERS AND SENSOR CONFIGURATION

Electromagnetic sounders with capabilities for deep sounding (many kilometers) of terrestrial ice sheets from airborne platforms have been built by a number of researchers. In the case of a cometary nucleus sounder, the main constraints are the power available and the weight limitation.

A summary of the parameters of a point design sounder are given in Table 4-1. These parameters correspond to a very realistic system compatible with spacecraft requirements and high quality information return. The selection of these parameters was a result of the following trade-offs:

(1) As discussed in Section III, the optimum frequency band for sounding the nucleus is between 30 and 100 MHz. A point design frequency of 40 MHz was selected. Much higher frequencies were avoided because of the fact that if rocky debris of a fraction of a meter size are imbedded in the icy nucleus, they would appreciably scatter waves at higher frequency, and therefore limit the sounding depth.

(2) A high peak power is desirable because it would allow sounding while the spacecraft is still at a large distance from the nucleus (see below). A peak power of 500 W was selected. Such a power can be achieved with present-day solid-state transmitters.

(3) The bandwidth was selected to achieve a range resolution capability of better than 45 m inside the nucleus. Better resolution can be easily achieved.

Based on these parameters, the operating range of the sounder (i.e., maximum distance between the nucleus and the spacecraft) can then be derived. It is reasonable to impose a requirement that the echo from the front surface must be 60 dB above the noise (i.e., SNR = 60 dB). Based on this requirement, the radar equation for specular return gives

$$d = \frac{G\lambda}{8\pi}\sqrt{\frac{rP_r}{kTB}} \approx 200 \text{ km}$$

where r is the Fresnel reflectivity of the surface and k is the Boltzmann constant.

The above point design system is capable of sounding an ice nucleus from any distance less than 140 km away. A higher SNR can also be achieved by pulse compression or incoherent addition of successive pulses. Evidently, for a nucleus with dirty ice, closer distance is required.

A block diagram of the point design sounder is shown in Figure 5-1. The sounder is essentially a pulsed radar system operating in the lower portion of the high frequency radio spectrum. The system consists of six subsystems which are as follows:

(1) Transmitter
(2) Receiver
(3) Timing Control
(4) Data Processing
(5) Power Supply and Switching
(6) Antenna, Matching, and TR Switching

The transmitter transmits a pulse of known frequency at some pulse duration and repetition rate. After the pulse is transmitted, the returning echo is received and transformed to a convenient intermediate frequency. The signal is amplified, envelope detected, and processed through a data processing system and stored for transmission to Earth via spacecraft radio.

The timing control circuitry insures that the transmit-receive (TR) switch is in the transmit mode when a pulse is about to be sent, and in the receive mode when a returning echo appears at the antenna. It also controls the IF amplifier gain such that gain increases as a function of time after the transmitted pulse is sent.

The data processing system processes the video signals containing the echo information into a form suitable for retransmission back to Earth. The power supply and interface contain all of the peripheral components which, though necessary for proper operation of the system, do not belong to any one subsystem. These include items such as the power supplies, telemetry for systems monitoring, command telemetry band switching, decoupling and packaging.

The antenna subsystem contains the antenna associated matching network, as well as deployment devices and the TR switch. A detailed description of the main subsystems follows.

A. TRANSMITTER

1. Master Oscillator (MO)

The master oscillator is the single source of frequency generation and timing control for the entire system. It is a fixed-frequency, crystal-controlled, temperature-compensated type capable of at least 1-mW output. The unit also exhibits good aging (long-term stability) characteristics and frequency stability without regard to supply voltage or temperatures existing in a spacecraft environment. Commercially available units exist which would fulfill this requirement.

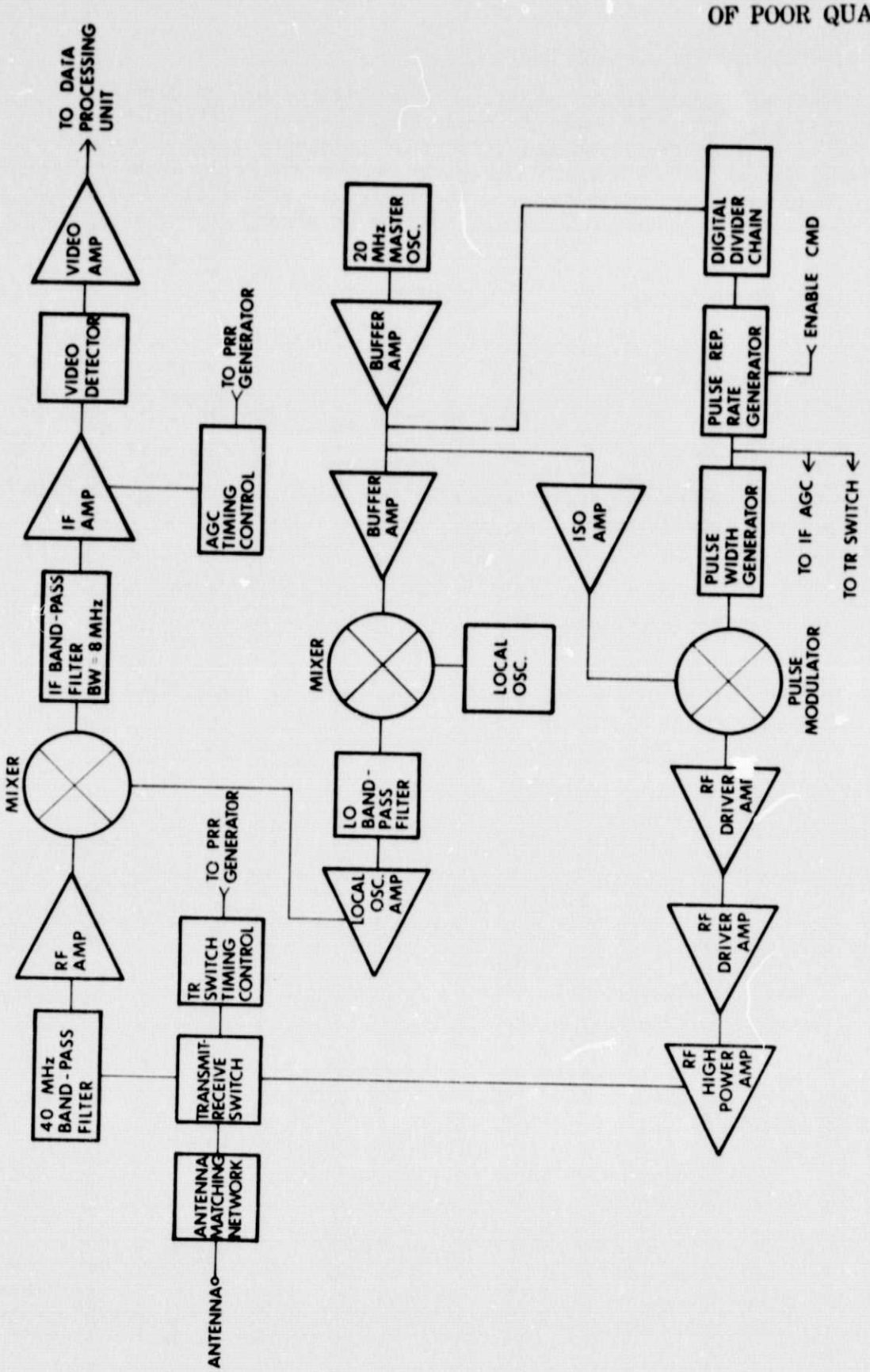

Figure 5-1. Block Diagram of the Point Design Sounder

2. Buffer Amp

The oscillator buffer amplifier provides the master oscillator with isolation from the rest of the system, insuring a stable master frequency source, free from the effects of frequency "pulling" which could occur during periods of peak power supply demands. This unit also provides a nominal power gain to offset the effect of driving the digital divider chain and local oscillator mixer.

3. Second Buffer Amp

The second buffer amp amplifies the output of the first buffer amp to a level sufficient to drive the local oscillator mixer (7 dB).

4. Isolation Amp

The isolation amplifier amplifies the output of the first buffer amp (or frequency divider) to a level necessary to drive the pulse modulator.

5. Digital Divider Chain (DPD)

The digital divider chain is clocked by a portion of the first buffer amp output. It divides the 20 MHz clock by 2×10^5 resulting in an output of 100 pulses/s.

6. Pulse Repetition Rate Generator (PRR)

The pulse repetition rate generator is a divider ($\div 10$) which, when enabled by a command pulse, fires the pulse width generator. It also provides timing pulses to the TR switch timing control and AGC timing control alerting those units that a pulse is about to be sent or received.

7. Pulse Width Generator (PWG)

The pulse width generator clocks the pulse modulator for a precise length of time allowing it to transmit the carrier frequency to the pulse modulator input.

8. Pulse Modulator (PM)

The pulse modulator is a double-balanced mixer (DBM) which is utilized as a low-level modulator. It accepts the TTL digital level source from the PWG and carrier frequency from the ISO amp. It outputs the carrier frequency to drive the first RF driver amp only when a pulse is available at the mixer input. The output is approximately -3 dB.

9. First Driver Amp (DA1)

The first driver amp is sourced from the PM output. It provides about 25 dB gain, giving an output of approximately 22 dBm which drives the second driver amp.

10. Second Driver Amp (DA2)

The second driver amp is a class "C" amplifier with 25 dB gain. Class "C" operation gives a much higher power efficiency since it is biased off during quiescent operation. The power output is approximately 50-W peak.

11. RF Power Amp (PA)

The RF power amp is the final power amplifier. It is a class "C" biased amplifier requiring 50-W drive and having an output of 500-W peak (gain = 10 dB). Solid-state design is used to eliminate the requirement for high-voltage power supplies. The output of the amplifier is fed directly to the TR switch to the antenna.

b. RECEIVER (RX)

1. Input Filter (BP1)

The input filter is located immediately after the TR switch. It receives the broadband RF noise and signal from the antenna. The bandwidth is sufficient to pass the desired returning echo of the transmitted pulse and reject the unwanted image frequency and broadband noise. The output directly feeds the RF amplifier. Addition of this filter increases the absolute sensitivity of the system but also adds directly to the noise figure of the system. The loss is expected to be less than 1.5 dB.

2. RF Amplifier (RF1)

The RF amplifier is a solid-state broadband design with wide dynamic range (80 dB). The nominal gain is approximately 14 dB and noise figure of 4 dB.

3. First Mixer (MX1)

The first mixer is a double-balanced broadband type which provides superior isolation. The RF output of the RF1 amplifier is mixed with the local oscillator and the difference product at the mixer output is selected as the IF frequency.

4. IF Filters (FF)

There is an IF filter at the carrier frequency with an 8 MHz bandwidth.

5. IF Amplifier (IFA)

The IF amplifier provides 80 dB amplification of the IF signal to the video. Provisions for 60 dB of gain control are included. Amplifier bandwidth (3 dB) is 10 MHz and IF frequency is 30 MHz. A video detector and video amplifier are also incorporated into the design. Video amp gain is 10 dB giving a total of 90 dB signal gain from the IF input.

6. AGC Timing Control (AGC)

AGC timing control is provided to vary the IF gain as a function of time so that the video level will remain constant with echo range.

7. Second Mixer (MX2)

The second mixer is a double-balanced type. This mixer adds the local oscillator frequency to the carrier frequency to generate a mixing frequency for MX1. Its high isolation provides 30 dB suppression of the local oscillator signal.

8. Local Oscillator (LO)

The local oscillator is a stable crystal oscillator type with sufficient output to drive MX2 (approximately equals 7 dBm). The frequency is the same as the IF frequency.

9. LO Bandpass Filter (LOF)

The local oscillator bandpass filter will have narrow selectivity and high shape factor. This is to insure that no unwanted mixer output product passes. Unwanted products are expected to down 30 dB through this device.

10. Local Oscillator Amp (LOA)

The local oscillator amp amplifies the filtered output of MX2 to provide sufficient power to drive MX1.

C. ANTENNA, MATCHING, AND SWITCHING (AMS)

1. TR Switch (TR)

The transmit-receive switch selects either the transmitter output or receiver input to the antenna. Isolation should be 60 dB to provide sufficient protection to the receiver input and allow RFA to recover quickly enough to receive the returning echo. Switching time should be to 100 ns.

2. Switch Timing Control (STC)

The switch timing control is used to control the TR. It must activate the switch fast enough to insure that no part of the transmitted pulse enters the receiver directly from the transmitter.

3. Antenna Matching Network (AMN)

The antenna matching network transfers the maximum amount of power to the antenna through a tuning network and Balun transformers.

SECTION VI

CONCLUSION

The potential significance of science returns from deep sounding of a cometary nucleus is very high. Electromagnetic echoes returned from the comet can be interpreted to deduce the internal structure of the nucleus. The cometary plasma places a lower bound of 10 MHz on the sounding frequency; ice absorption requires the frequency to be below 100 MHz for deep penetration.

Radiation scatters back to the antenna by a variety of mechanisms; the most important are reflection from layered dielectric interfaces and inhomogeneities, and radiation refracted through the nucleus. The strength of these signals and their time delays yield a profile of the dielectric changes throughout the nucleus.

A point design sounder which can operate from a 140-km distance at 40 MHz is discussed in some detail and found to be within the current state-of-the-art of space technology.

In conclusion, a sounder can be developed for the payload of a rendezvous comet mission, and its scientific payoff is appreciable. It is basically the only sensor which can accurately determine the complete internal structure of the nucleus.

REFERENCES

Report of the Comet Halley Science Working Group, NASA TM 78420, National Aeronautics and Space Administration, Washington, D.C., July 1977.

Born, M. and E. Wolf, Principles of Optics, Pergamon, Bath, England, 1965.

Battan, L., Radar Meteorology, University Chicago Press, Chicago, 1959.

Evans, S., "Dielectric Properties of Ice and Snow -- A Review," J. Glaciology, Vol. 5, No. 42, p. 773, 1964.

Feldman, P. D., "The Composition of Comets," Am. Sci., p. 299, May - June 1977.

Gudmandsen, P., "Layer Echoes in Polar Ice Sheets," J. Glaciology, 15, p. 95, 1975.

Gudmandsen, P., Studies of Ice by Means of Radio Echo Sounding, Report R162, Technical University of Denmark, Lyngby, 1976.

Hoekstra, P. and P. Cappillino, "Dielectric Properties of Sea and Sodium Chloride Ice at UHF and Microwave Frequencies," J. Geophys. Res., Vol. 76, No. 20, p. 4922, July 1971.

Ip, W. H. and D. A. Mendis, "The Structure of Cometary Ionospheres," Icarus, 28, p. 389, 1976.

Robin, G. De Q., S. Evans and J. T. Bailey, "Interpretation of Radio Echo Sounding in Polar Ice Sheets," Phil. Trans. Roy. Soc. London, Vol. 265, p. 437, December 1969.

Smith, W. and S. Evans, J. Sci. Inst. (formerly J. Phys. E.), Ser. Z, Vol. 2, pp. 131-136, 1969.

Von Hippel, A., Dielectrics and Waves, John Wiley, New York, 1954.

Westphal, W. B., Private Communication.

Whippel, F. L., Astrophys. J., III, p. 375, 1950.

Whipple, F. L. and W. F. Heubner, "Physical Processes in Comets," Ann. Res. Astron. and Astrosphys., p. 143, 1976.